SUBFUNCTIONALIZATION OF ENDONUCLEASE G ISOZYMES IN *XENOPUS TROPICALIS*

Natsuki Sou[1] and Alexander A. Tokmakov[1]

Abstract

Endonuclease G (EndoG) is known to be involved in apoptotic degradation of nuclear DNA. It has also been proposed to carry out mRNA degradation in the cytoplasm of apoptotic cells. In the present work, predictive bioinformatics analysis and comparative homology modeling were used to reveal subfunctionalization of two EndoG isozymes (*xt*EndoG) in the *Xenopus tropicalis* western clawed frog. The analysis suggests that mitochondrial translocation of one of these proteins can be regulated by calcium-dependent phosphorylation in the region of its N-terminal signal sequence. Detailed comparison of modeled 3D structures of the two proteins reveals thermodynamic and structural differences that affect local protein stability. Our findings bring to light a novel mechanism that can possibly regulate mitochondrial translocation of EndoG and provide a rationale for the existence of two highly homologous *xt*EndoG proteins in *Xenopus tropicalis*. Here, we also discuss a probable involvement of the calcium-dependent mechanism of EndoG translocation in frog egg apoptosis.

Key words: endonuclease G, homology modeling, predictive bioinformatics, *Xenopus tropicalis*,

Introduction

Endonuclease G (EndoG) is a nuclear-encoded DNA/RNA nonspecific nuclease found in the mitochondria of eukaryotic cells. It is involved in the regulation of mitochondrial DNA (mtDNA) and has been associated with apoptosis (programmed cell death) and other cellular processes. The enzyme is released from mitochondria upon induction of apoptosis together with cytochrome *c* and other proapoptotic proteins (Parrish et al. [(1)], van Loo et al. [(2)]). After its release from mitochondria, EndoG is translocated into the nucleus, where it degrades chromosomal DNA (Parrish et al. [(1)], Li et al. [(3)]). In addition, it is suggested that EndoG may also cleave cytoplasmic mRNA (Del Prete et al. [(4)], Kalinowska et al. [(5)], Tokmakov et al. [(6)]). Crystal structures of several EndoG proteins from different species have been resolved and deposited in the Protein Data Bank (Loll et al. [(7)], Lin et al. [(8)], Park et al. [(9)]). They helped to clarify catalytic and regulatory mechanisms of the enzyme. The EndoG protein was found to possess an N-terminal mitochondrial targeting sequence or mitochondrial localization signal that directs the protein to mitochondria. The N-terminal mitochondrial targeting sequence is essential for proper localization and function of EndoG within this organelle (Schäfer et al. [(10)]).

Multiple EndoG proteins have been identified in different species and different cell types. However, only limited information is currently available about the specific EndoG isoforms in the Western clawed frog *Xenopus tropicalis*. This animal represents a conventional experimental model for studies in developmental biology and reproduction. The complete genome of this species has been sequenced and annotated (Hellsten et al. [(11)]).

In the present work, we investigated the presence of multiple isoforms of EndoG in *Xenopus tropicalis* and the extent to which these isoforms have undergone subfunctionalization, the process by which different isoforms of a gene or protein evolve distinct functions (Force et al. [(12)]). Considering predominantly mitochondrial localization of this protein, we have focused on probable regulation of EndoG translocation by phosphorylation. At present, the specific mechanisms governing mitochondrial translocation of EndoG have not been well-investigated, and the involvement of phosphorylation in its mitochondrial translocation has not been demonstrated. However, it is known that intracellular localization of multiple proteins can be regulated by phosphorylation (Schmidt et al. [(13)]). Particularly, phosphorylation of N-terminal mitochondrial targeting sequences can modulate their interaction with the cell membrane and/or import machinery, affecting the efficiency of protein import into mitochondria.

Received 25 December 2023

[1] Institute of Advanced Technology, Faculty of Biology-Oriented Science and Technology, KinDai University, 930 Nishimitani, Kinokawa city, Wakayama 649-6493, Japan

Our current study based on predictive bioinformatics analysis and comparative homology structural modeling reveals the existence of two EndoG isozymes in *Xenopus tropicalis.* Detailed comparison of their sequences and 3D-structures provides a rationale for the existence of these highly homologous proteins and proposes a calcium- and phosphorylation-dependent mechanism of EndoG translocation, engaged, presumably, in frog egg apoptosis.

Materials and methods

Sequence retrieval and alignment

Amino acid sequences of *X. tropicalis* endonuclease G (*xt*EndoG) were retrieved from the NCBI protein database (https://www.ncbi.nlm.nih.gov/). The annotated amino acid *sequence of mouse EndoG (accession number* NP_031957.1) *was used as a query sequence* to search a database of *X. tropicalis* proteins using the The *Basic Local Alignment Search Tool,* BLAST, (https://blast.ncbi.nlm.nih.gov/Blast.cgi). Sequence alignments were performed using the pairwise Global Alignment BLAST tool and the CLUSTALW (Thompson et al. [14], http://www.ch.embnet.org/software/ClustalW.html).

Prediction of secondary structure, signal peptides and phosphorylation sites

Secondary structure predictions for the N-terminal regions of *xt*EndoG proteins were carried out using the GOR4 tool (Kouza et al. [15], https://npsa-pbil.ibcp.fr/cgi-bin/npsa_automat.pl?page=/NPSA/npsa_gor4.html). Signal sequences were identified with the SignalIP-4.1 tool that predicts the presence of signal peptides and location of cleavage sites (Nielsen [16], https://services.healthtech.dtu.dk/services/SignalP-4.1/). Phosphorylation sites were predicted using the sequence-based phosphorylation prediction server NetPhos-3.1 utilizing ensembles of neural networks (Blom et al. [17], https://services.healthtech.dtu.dk/services/NetPhos-3.1/).

Homology modeling

The three-dimensional structures of *xt*EndoG isozymes were built by homology modeling based on the crystal structure of a mammalian protein. The crystal structure of mouse EndoG at a resolution of 2.80 Å was used as a template structure to generate the 3D models of *xt*EndoGs (Park et al. [9]). The template protein was crystallized in a DNA-free form. The coordinate file of the template was retrieved from the Protein Data Bank (PDB: 6lyf2.A). Homology modeling was carried out using the protein structure homology modeling server SWISS-MODEL (Guex and Peitsch [18], Schwede et al. [19], http://swissmodel.expasy.org/). Visualization of the modeled *xt*EndoG structures was done with the commercial molecular graphics software Waals (Altif Laboratories, Tokyo, Japan) and DeepView/Swiss-Pdb Viewer (Guex and Peitsch [18], https://spdbv.unil.ch/).

Other methods

Energy computations were carried out with the GROMOS96 implementation of Swiss-Pdb Viewer. Superposition of the *xt*EndoG structures and calculation of superposition RMSDs was done using “Autofit” function of the Waals software. Discerning of ligand binding pockets in EndoG was conducted with the protein-ligand binding site prediction tool P2RANK (Jendele et al. [20], https://prankweb.cz/).

Results and discussion

The family of EndoG proteins in *Xenopus tropicalis*

Several statistically significant BLAST hits were obtained using the published sequence of mouse Endo G protein as a bait. Out of them, the top two hits, NP_001017202.1 and KAE8584272.1, had the BLAST score above 200 and covered the full-length protein containing 293 amino acids. Starting from the third hit, exonuclease G and endonuclease domain-containing proteins of low sequence coverage and homology were pinpointed by BLAST. The distribution of the top BLAST hits on subject sequences is presented in Fig. 1. The identity of the top two hits as EndoG proteins was confirmed using the UniProt database (data not shown). Thus, we concluded that the complete family of EndoG proteins in *Xenopus tropicalis* consists of two members. Their sequences were aligned using ClustalW, and the alignment is presented in Fig. 2. The sequence differences included three amino acid substitutions in the N-terminal region and one substitution in the catalytic protein core. Potential implications of these differences for regulation and function of the two proteins were further investigated.

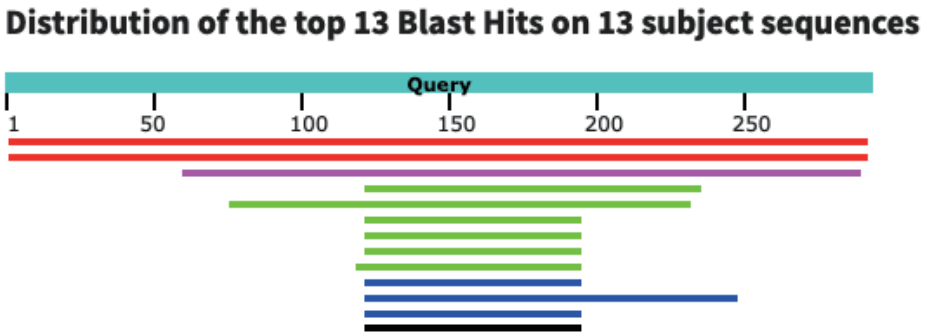

Fig 1. Graphic summary of the BLAST search for *Xenopus tropicalis* EndoG. Sequence coloring corresponds to different homology scores from high (red) to low (black).

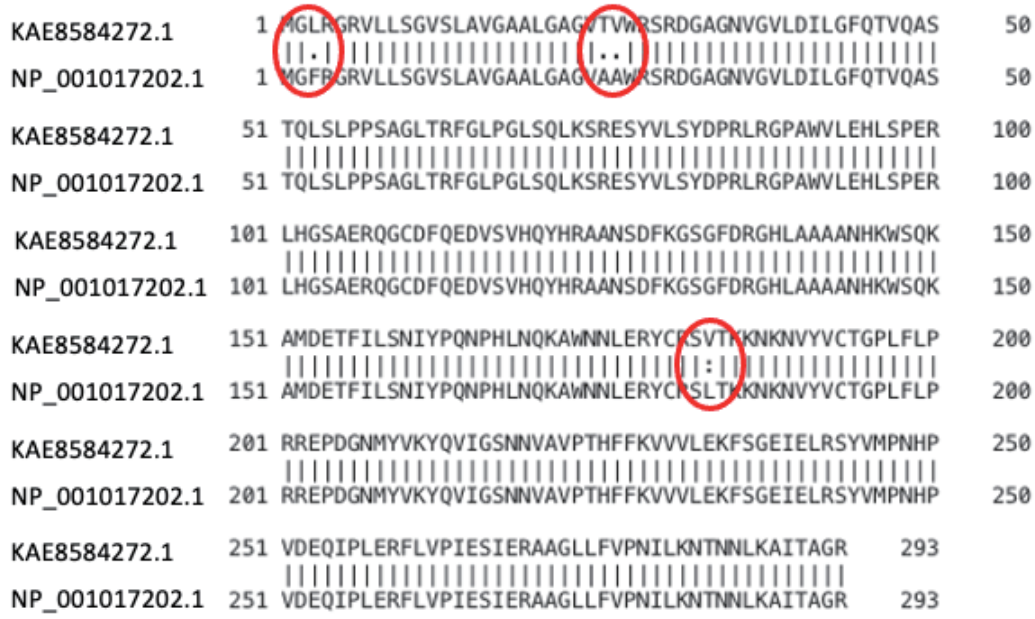

Fig 2. Sequence alignment of *xt*EndoGs. Non-identical amino acids are encircled.

Secondary structure and signal peptide predictions for the N-terminal regions

Amino acid sequences of the two *xt*EndoG isoforms differed in their N-terminal region. Secondary structure predictions performed with the use of the GOR4 prediction algorithm indicated the presence of alpha-helical structures in this region. Importantly, alpha-helical propensity of NP_001017202.1 was much higher than that of KAE8584272.1: alpha-helical conformation was predicted in 16 vs 6 residues of their respective N-terminals (Fig. 3A,B). Apparently, the three N-terminal amino acid substitutions should be related to this structural difference. The next section of this paper identifies T25 as a key residue affecting formation of the helical structure and mitochondrial translocation of *xt*EndoG. As the N-terminal of EndoG is known to comprise the mitochondrial localization signal, next we determined the probability of a signal peptide sequence in this region using SignalP-4.0 server. The isoform with a greater length of alpha-helical structure, NP_001017202.1, was predicted to contain the signal peptide and cleavage site between positions 20 and 21 with the high probability of 0.657. A much lower probability of the signal peptide and cleavage site (D=0.392) was predicted for KAE8584272.1 (Fig. 3C). These results suggest that the NP_001017202.1 protein is translocated and processed into the mitochondrial compartment, whereas KAE8584272.1 should be retained in the cytoplasm.

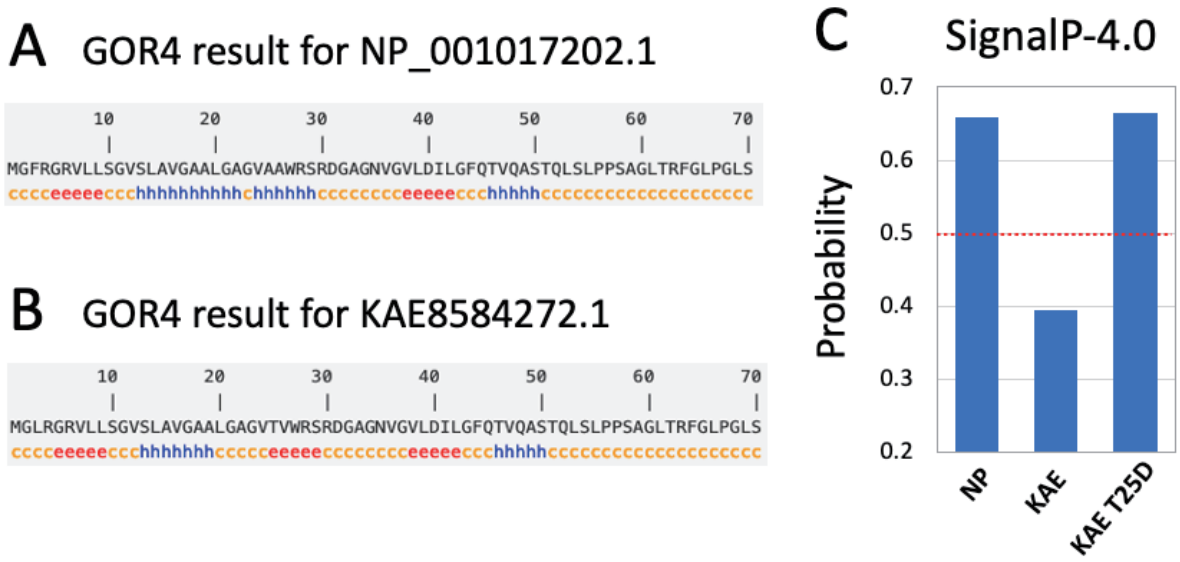

Fig 3. Prediction of secondary structure and signal peptides in *xt*EndoGs. Panels **A** and **B** show secondary structure predictions for the two *xt*EndoG proteins, where h denotes alpha-helix, e – beta-sheet, and c – random coil. Probability of a signal peptide is presented in panel **C**.

Calcium-dependent translocation of KAE8584272.1 isoform

Notably, the KAE8584272.1 isoform retained in the cytoplasmic compartment contains A25T substitution in its N-terminal (Fig. 2). It is well established that threonine is efficiently phosphorylated in different proteins by various protein kinases. Therefore, next we investigated whether T25 of KAE8584272.1 can be phosphorylated too. Several phosphorylation sites were predicted to reside within the N-terminal region of this protein, and among them T25 displayed the highest potential for phosphorylation (Fig. 4A). The greatest probability of T25 phosphorylation (0.732) was predicted for PKC protein kinase (PKC) using the NetPhos-3.1 phosphorylation prediction server (Fig. 4B).

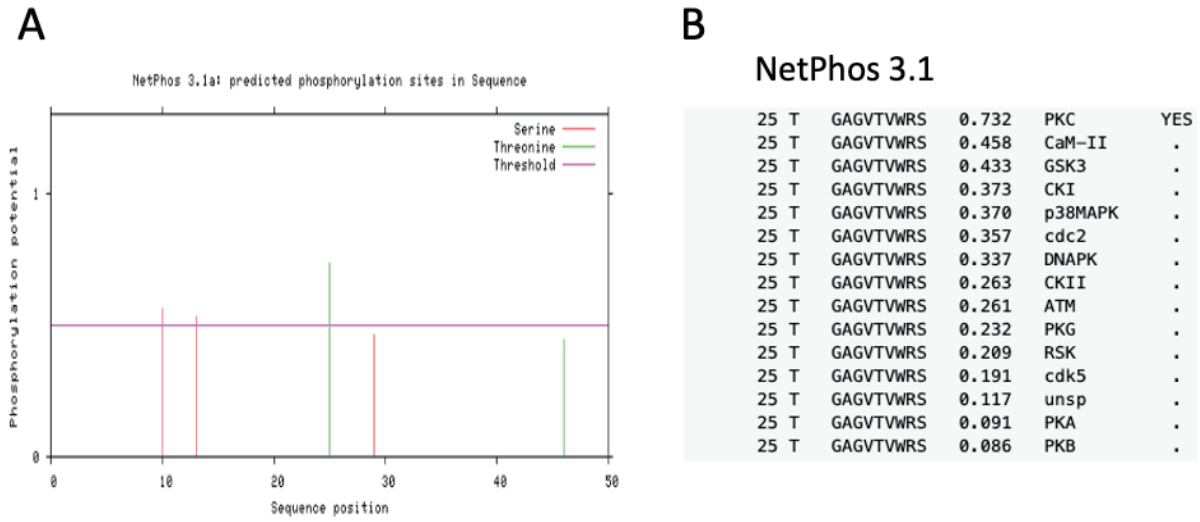

Fig 4. Prediction of phosphorylation sites in the KAE8584272.1 protein. Phosphorylation sites were predicted using the internet-based NetPhos-3.1 tool. Panel **A** reveals the presence of phosphorylation sites in the N-terminal region of the protein, and panel **B** presents probability scores for T25 phosphorylation by different protein kinases.

The value exceeded the prognostic threshold of 0.5, however, other protein kinases have also been identified that could phosphorylate this residue with a considerably lower probability. Among them, CaM-II (calcium/calmodulin-dependent kinase II) followed PKC by the probability score for T25 phosphorylation. Thus, the two top kinases that can phosphorylate T25 of the KAE8584272.1 protein with the highest probability, PKC and CaM-II, are calcium-dependent protein kinases. Remarkably, T25D mutant, which mimics T25-phosphorylated KAE8584272.1,

was predicted to contain the signal peptide and cleavage site between positions 20 and 21 with the high probability of 0.663 (Fig. 3C) on par with NP_001017202.1. The results presented in this section suggest that KAE8584272.1 protein can be efficiently translocated and processed into the mitochondrial compartment after calcium-dependent phosphorylation on T25. Probable involvement of calcium-dependent translocation in the apoptotic function of EndoG is further commented upon in the "Conclusions" section.

Structural homology modeling of *xt*EndoG

To estimate implications of L183V substitution in the catalytic core of *xt*EndoG (Fig. 2), homology modeling of 3D protein structures was carried out for the two isozymes using the SWISS MODEL server. The crystal structure of mouse EndoG (PDB entry, 6lyf), which covered 73.53% of *X. tropicalis* sequence, was used as a template for homology modeling. Notably, the N-terminal tail (first 44 amino acids) was truncated in the deposited crystal structure of the template protein, and the N-terminus of *xt*EndoG could not be modeled by this approach. The generated models of *xt*EndoG were validated using QMEAN, GMQE, and Ramachandran plots (Fig. 5). These methods verified folding integrities of the generated 3D models and confirmed their quality. The generated 3D structure of NP_001017202.1 is presented in Fig. 6A, and it has a good overall structural alignment with the modelled structure of KAE8584272.1 (see next section for details). The structure covers the entire catalytic core of the protein, lacking the long and largely unstructured N-terminal discussed in previous sections. Notably, a long amphipathic alpha-helix separates the site of L183V substitution from the DNA- and magnesium-binding catalytic center (Fig. 6). It appears, that the L183V substitution is located in the region of elevated spatial uncertainty, as judged from the representation of the SWISS MODEL stability factor, which reflects the atomic displacement parameter or B-factor (Fig. 6B).

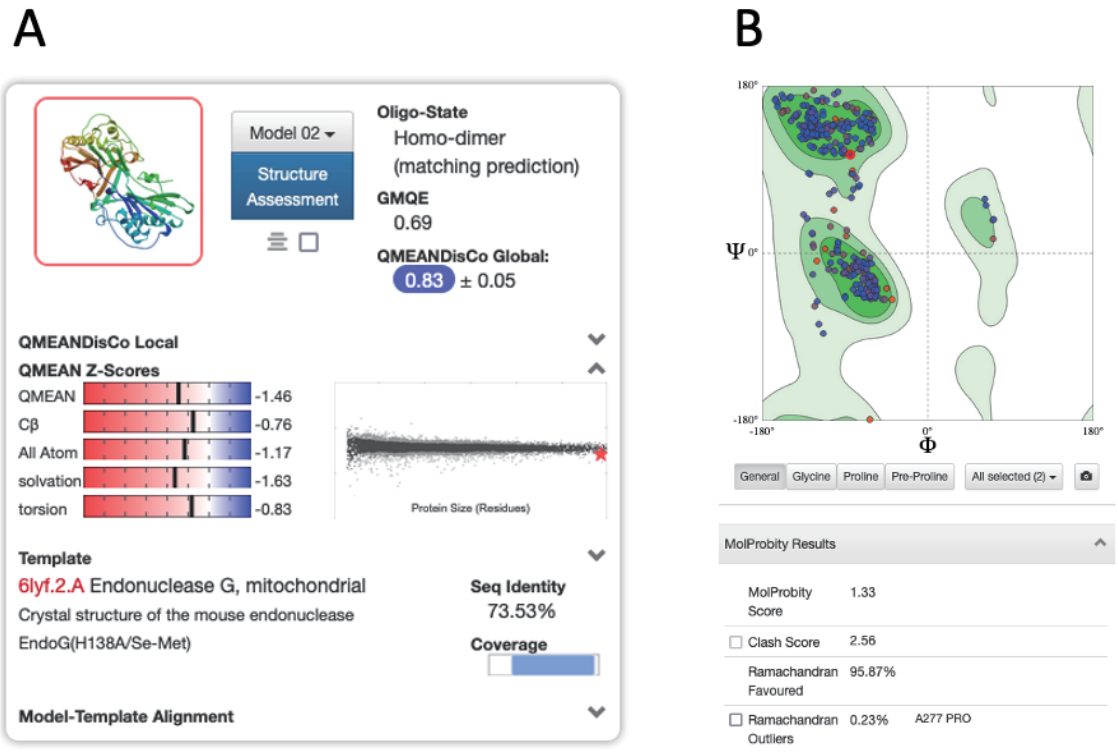

Fig 5. Validation of generated *xt*EndoG models using QMEAN analysis (A) and Ramachandran plot (B).

Superimposition of *xt*EndoG structures

Spatial superposition of the two protein molecules was performed using the AutoFit mode of the Waals molecular viewer. The modeled structures superimposed remarkably well, with an RMSD value of just 0.009Å over the whole 218 residues of the molecular core (Fig. 7A, Table 1). In fact, only nine amino acids (179-184 and 189-191) located in the region of L183V substitution were displaced in the two proteins with the RMSD values ranging from 0.01 to 0.07 Å (Table 1). The most affected amino acids with the highest RMSDs included hydrophobic residues Cys180 and Val190 located in the close vicinity of the substitution site (Table 1, Fig. 7B).

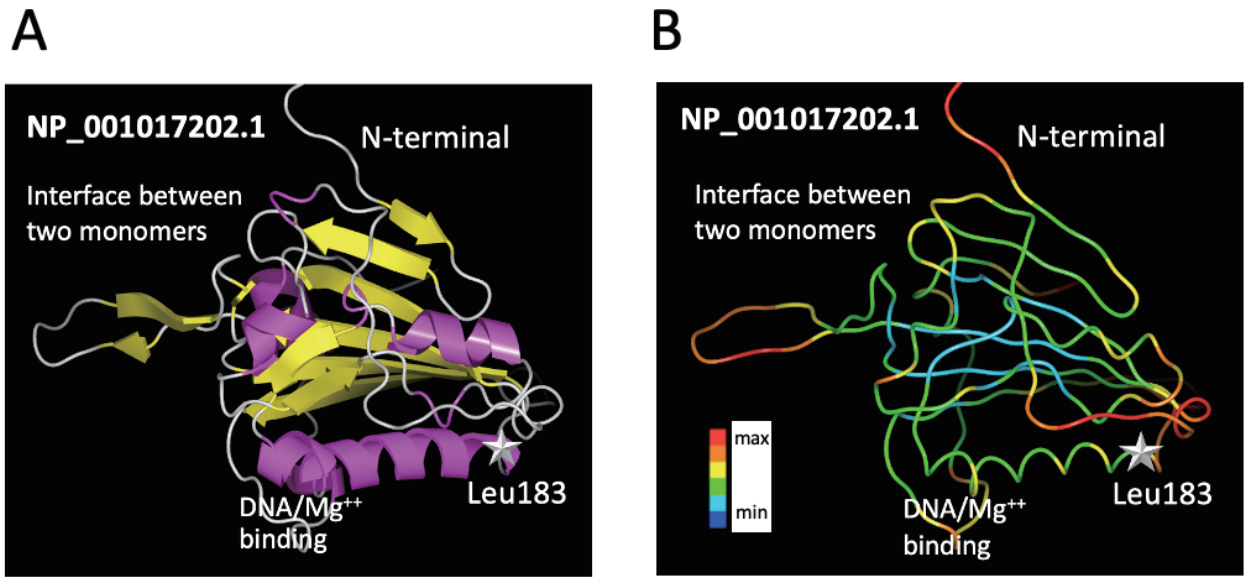

Fig 6. Modeled 3D structure of the NP_001017202.1 protein. Cartoon representation and stability factor coloring for the protein catalytic core are shown in panels A and B, respectively.

Table 1 RMSDs for the superimposed models of *xtEndoG* (218 residues, RMSD=0.009Å)

A	128	129	130	131	132	133	134	135	136	137	138	139	140	141	142	143	144	145	146	147	148	149	150	151	152	153	154	155	156	157	158	159	160
	D	F	K	G	S	G	F	D	R	G	H	L	A	A	A	A	N	H	K	W	S	Q	K	A	M	D	E	T	F	I	L	S	N
	D	F	K	G	S	G	F	D	R	G	H	L	A	A	A	A	N	H	K	W	S	Q	K	A	M	D	E	T	F	I	L	S	N
A	128	129	130	131	132	133	134	135	136	137	138	139	140	141	142	143	144	145	146	147	148	149	150	151	152	153	154	155	156	157	158	159	160
	0.00		0.00		0.00		0.00		0.00		0.00		0.00		0.00		0.00		0.00		0.00		0.00		0.00		0.00		0.00		0.00		0.00
		0.00		0.00		0.00		0.00		0.01		0.00		0.00		0.00		0.00		0.00		0.00		0.00		0.00		0.00		0.00		0.01	

A	161	162	163	164	165	166	167	168	169	170	171	172	173	174	175	176	177	178	179	180	181	182	183	184	185	186	187	188	189	190	191	192	193
	I	Y	P	Q	N	P	H	L	N	Q	K	A	W	N	N	L	E	R	Y	C	R	S	L	T	K	K	N	K	N	V	Y	V	C
	I	Y	P	Q	N	P	H	L	N	Q	K	A	W	N	N	L	E	R	Y	C	R	S	V	T	K	K	N	K	N	V	Y	V	C
A	161	162	163	164	165	166	167	168	169	170	171	172	173	174	175	176	177	178	179	180	181	182	183	184	185	186	187	188	189	190	191	192	193
	0.00		0.00		0.00		0.00		0.00		0.00		0.00		0.00		0.00		0.01		0.05		0.06		0.00		0.00		0.01		0.02		0.00
		0.01		0.00		0.00		0.00		0.00		0.00		0.00		0.00		0.00		0.07		0.01		0.02		0.00		0.00		0.06		0.00	

A	194	195	196	197	198	199	200	201	202	203	204	205	206	207	208	209	210	211	212	213	214	215	216	217	218	219	220	221	222	223	224	225	226
	T	G	P	L	F	L	P	R	R	E	P	D	G	N	M	Y	V	K	Y	Q	V	I	G	S	N	N	V	A	V	P	T	H	F
	T	G	P	L	F	L	P	R	R	E	P	D	G	N	M	Y	V	K	Y	Q	V	I	G	S	N	N	V	A	V	P	T	H	F
A	194	195	196	197	198	199	200	201	202	203	204	205	206	207	208	209	210	211	212	213	214	215	216	217	218	219	220	221	222	223	224	225	226
	0.00		0.00		0.00		0.00		0.00		0.00		0.00		0.00		0.00		0.00		0.00		0.00		0.00		0.00		0.00		0.00		0.00
		0.00		0.00		0.00		0.00		0.01		0.00		0.00		0.00		0.00		0.00		0.00		0.00		0.00		0.00		0.00		0.00	

Calculation of interaction energies in the region of L183V substitution revealed that Leu183 in NP_001017202.1 has a lower total energy than Val183 in KAE8584272.1 (-54.373 vs -36.411 kJ/mol), mainly, due to the decrease in the non-Bonded energy component (Table 2). Moreover, Cys180 and Val190, as well as the whole region affected by the L183V substitution (residues 179-191), displayed lower interaction energies in NP_001017202.1 than in KAE8584272.1 (Table 2). Thus, it can be concluded that a longer aliphatic side chain of Leu183 promotes stronger hydrophobic interactions with the neighboring hydrophobic residues, such as Cys180 and Val190, than that of Val183 (Fig. 7B). The stronger interactions reduce total interaction energy of this region, resulting in its increased stability and decreased flexibility. It is not apparent, however, how the decreased flexibility of this region can affect the remote catalytic site and enzymatic activity of *xt*EndoG. Moreover, the exceptionally low whole-length RMSD value (0.009A) points to the absence of a long-range impact of the core substitution on the positions of distant residues and, therefore, on the overall structure of the protein molecule (Table 1, Fig. 7A). Thus, it is highly unlikely that this substitution elicits any allosteric effects.

The region of core substitution evades intermolecular interactions

Regarding the improbable direct effect of the L183V substitution on the distant catalytic site of *xt*EndoG, we have sought other explanation for evolutionary conservation of this mutation and suggested that the substitution region might be involved in intermolecular interactions with small chemical ligands or large protein molecules.

Table 2 Interaction energies in the region of L183V substitution

NP_001017202.1

residue	bonds	angles	torsion	improper	nonBonded	electrostatic	constraint //	TOTAL
TYR A 179	10.806	22.256	5.061	0.982	-45.16	-47.57	0.0000 // E=	-53.624
CYSH A 180	1.783	5.470	1.492	0.545	-40.13	-5.79	0.0000 // E=	-36.631
ARG A 181	4.275	14.778	10.177	0.103	-45.69	-256.23	0.0000 // E=	-272.587
SER A 182	3.422	6.921	6.574	1.659	-25.32	-17.84	0.0000 // E=	-24.581
LEU A 183	2.266	7.028	4.159	0.475	-47.03	-21.27	0.0000 // E=	-54.373
THR A 184	1.856	9.956	3.046	0.633	-36.71	-13.00	0.0000 // E=	-34.217
LYSH A 185	2.717	4.092	3.029	0.078	-20.95	6.75	0.0000 // E=	-4.291
LYSH A 186	2.972	5.090	3.729	0.107	-23.86	6.79	0.0000 // E=	-5.171
ASN A 187	4.466	7.337	4.548	0.010	-39.63	-165.38	0.0000 // E=	-188.656
LYSH A 188	2.076	5.822	1.129	0.533	-30.17	6.14	0.0000 // E=	-14.475
ASN A 189	3.795	5.005	6.707	0.806	-40.63	-169.61	0.0000 // E=	-193.937
VAL A 190	2.073	4.495	3.394	0.286	-35.40	-14.41	0.0000 // E=	-39.559
TYR A 191	10.560	23.117	4.621	0.379	-70.28	-56.09	0.0000 // E=	-87.693

KAE8584272.1

residue	bonds	angles	torsion	improper	nonBonded	electrostatic	constraint //	TOTAL
TYR A 179	11.300	22.013	5.244	1.018	-42.77	-48.94	0.0000 // E=	-52.137
CYSH A 180	2.031	6.442	1.091	0.246	-38.84	-5.07	0.0000 // E=	-34.106
ARG A 181	4.585	13.456	12.933	0.096	-44.84	-255.19	0.0000 // E=	-268.958
SER A 182	3.368	7.075	6.447	1.547	-24.92	-18.43	0.0000 // E=	-24.912
VAL A 183	2.683	7.098	2.012	1.009	-28.80	-20.41	0.0000 // E=	-36.411
THR A 184	1.802	11.393	3.052	0.701	-37.71	-12.99	0.0000 // E=	-33.751
LYSH A 185	2.757	4.023	3.000	0.090	-20.93	6.89	0.0000 // E=	-4.165
LYSH A 186	3.041	4.194	3.808	0.148	-23.08	6.20	0.0000 // E=	-5.690
ASN A 187	4.836	7.463	4.626	0.008	-39.18	-165.71	0.0000 // E=	-187.963
LYSH A 188	2.176	5.718	1.135	0.496	-30.22	6.14	0.0000 // E=	-14.560
ASN A 189	3.659	4.431	6.744	0.949	-39.88	-169.13	0.0000 // E=	-193.228
VAL A 190	3.202	4.505	2.977	0.082	-31.34	-13.38	0.0000 // E=	-33.962
TYR A 191	11.084	22.893	4.452	0.620	-70.06	-55.50	0.0000 // E=	-86.518

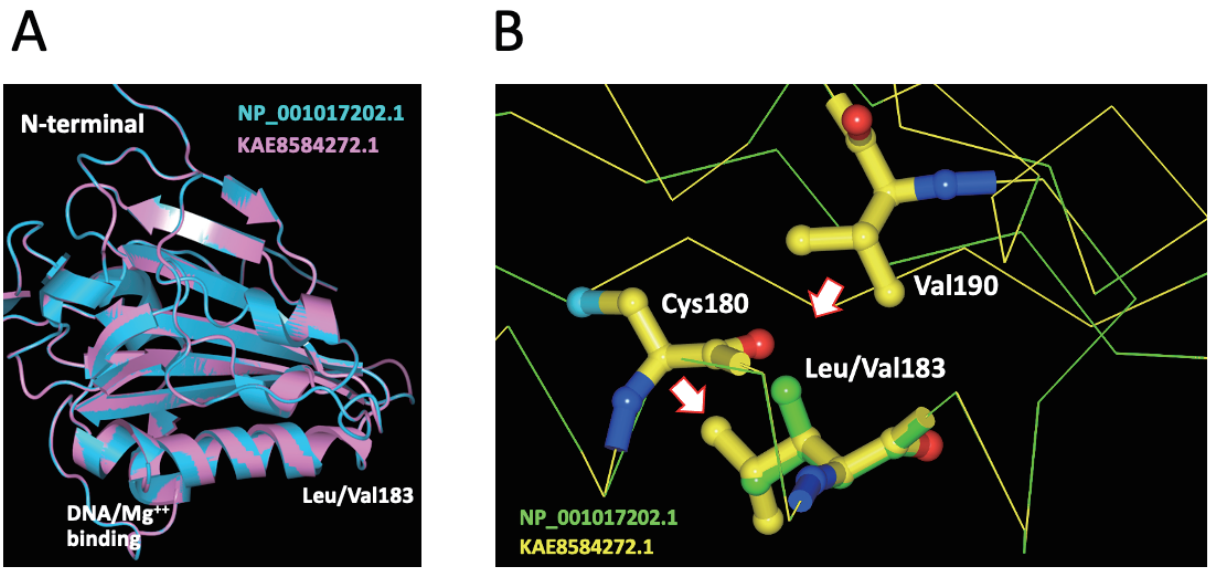

Fig 7. Superposition of *xt*EndoG models. Superpositions of the complete modeled regions **(A)** and the region of L183V substitution **(B)** are shown.

Bioinformatics prediction of ligand binding pockets using the P2RANK predictive tool revealed that the substitution site is located quite far from the closest identified ligand-binding pocket (Fig. 8A). Similarly, this site is not involved in the interaction of *xt*EndoG with a large inhibitor protein, as revealed by the resolved 3D structure of *Drosophila* EndoG complexed with the inhibitor domain of Ku 80 protein (Loll et al.[7], Fig. 8B). In fact, the side chain of homologous Leu201 in this structure faces the inner space of the EndoG molecule rather than the intermolecular niche. Thus, we conclude that it is unlikely that the L183V substitution site is involved in intermolecular interactions.

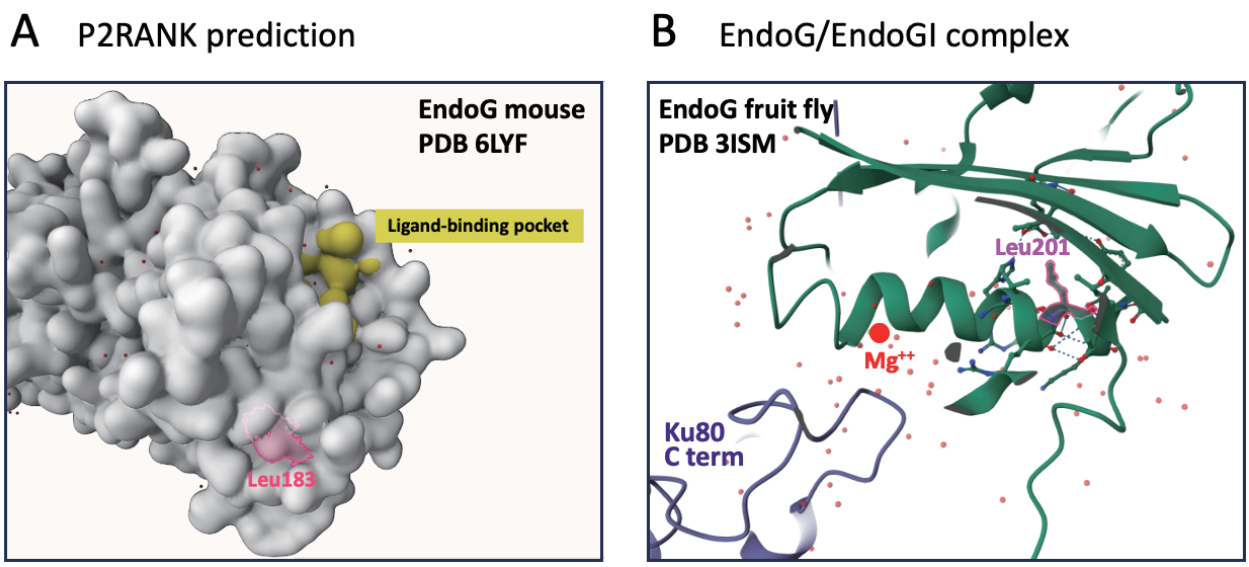

Fig. 8. Intermolecular interactions in the region of L183V substitution. Prediction of ligand binding pockets **(A)** and EndoG interaction with an inhibitor protein **(B)** are presented.

Conclusions

The complete EndoG family in *Xenopus tropicalis* consists of two highly homologous proteins. Their sequences differ by three amino acid substitutions in the N-terminal region and one substitution in the catalytic core. Bioinformatics analysis demonstrates that mitochondrial translocation of one of the isoforms can be regulated by calcium-dependent phosphorylation in the N-terminal mitochondrial targeting sequence. Considering that apoptosis is initiated in *Xenopus* eggs after the meiotic exit triggered by calcium signal (Tokmakov et al., [21] Iguchi et al. [22]), the revealed calcium-dependent and phosphorylation-mediated mechanism of EndoG translocation can be potentially involved in frog egg apoptosis. Enhanced translocation of EndoG into mitochondria at the initiation of the apoptotic process would allow accumulation of the processed and highly active form of the enzyme in the mitochondria before permeabilization of the mitochondrial outer membrane. This should increase the robustness of apoptosis when the enzyme is abundantly released from mitochondria. Furthermore, structural homology modeling reveals remarkably good superposition of the two modeled *xt*EndoG protein structures (RMSD=0.009Å) that display different local stability in the region of the core substitution L183V. However, it is unlikely that this substitution can affect the remote catalytic site and enzymatic activity of EndoG. In addition, it is improbable that the substitution region is involved in intermolecular interactions. Thus, the reason for evolutionary fixation of this mutation remains obscure and requires further investigation.

References

1. Parrish, J., Li, L., Klotz, K., Ledwich, D., Wang, X., & Xue, D. (2001) Mitochondrial endonuclease G is important for apoptosis in C. elegans. *Nature* **412**, 90–94.
2. van Loo, G., Schotte, P., van Gurp, M., Demol, H., Hoorelbeke, B., Gevaert, K., Rodriguez, I., Ruiz-Carrillo, A., Vandekerckhove, J., Declercq, W., Beyaert, R., & Vandenabeele, P. (2001) Endonuclease G: a mitochondrial protein released in apoptosis and involved in caspase-independent DNA degradation. *Cell Death Differ.* **8**, 1136–1142.
3. Li, L. Y., Luo, X., & Wang, X. (2001) Endonuclease G is an apoptotic DNase when released from mitochondria. *Nature* **412**, 95–99.
4. Del Prete, M. J., Robles, M. S., Guáo, A., Martínez-A, C., Izquierdo, M., & Garcia-Sanz, J. A. (2002) Degradation of cellular mRNA is a general early apoptosis-induced event. *FASEB J.* **16**, 2003–2005.
5. Kalinowska, M., Garncarz, W., Pietrowska, M., Garrard, W. T., & Widlak, P. (2005) Regulation of the human apoptotic DNase/RNase endonuclease G: involvement of Hsp70 and ATP. *Apoptosis* **10**, 821–830.
6. Tokmakov, A. A., Iguchi, S., Iwasaki, T., Fukami, Y., & Sato, K. I. (2017) Global decay of mRNA is a hallmark

of apoptosis in aging Xenopus eggs. *RNA biology* **14**, 339–346.
7. Loll, B., Gebhardt, M., Wahle, E., & Meinhart, A. (2009) Crystal structure of the EndoG/EndoGI complex: mechanism of EndoG inhibition. *Nucleic Acids Res.* **37**, 7312–7320.
8. Lin, J. L., Wu, C. C., Yang, W. Z., & Yuan, H. S. (2016) Crystal structure of endonuclease G in complex with DNA reveals how it nonspecifically degrades DNA as a homodimer. *Nucleic Acids Res.* **44**, 10480–10490.
9. Park, K. H., Yoon, S. M., Song, H. N., Yang, J. H., Ryu, S. E., & Woo, E. J. (2020) Crystal structure of the mouse endonuclease G. *Biochem. Biophys. Res. Commun.*, **526**, 35–40.
10. Schäfer, P., Scholz, S. R., Gimadutdinow, O., Cymerman, I. A., Bujnicki, J. M., Ruiz-Carrillo, A., Pingoud, A., & Meiss, G. (2004) Structural and functional characterization of mitochondrial EndoG, a sugar non-specific nuclease which plays an important role during apoptosis. *J. Mol. Biol.* **338**, 217–228.
11. Hellsten, U., Harland, R. M., Gilchrist, M. J., Hendrix, D., Jurka, J., Kapitonov, V., Ovcharenko, et al., (2010) The genome of the Western clawed frog Xenopus tropicalis. *Science* **328**, 633–636.
12. Force, A., Lynch, M., Pickett, F. B., Amores, A., Yan, Y. L., & Postlethwait, J. (1999) Preservation of duplicate genes by complementary, degenerative mutations. *Genetics* **151**, 1531–1545.
13. Schmidt, O., Harbauer, A. B., Rao, S., Eyrich, B., Zahedi, R. P., Stojanovski, D., Schönfisch, B., Guiard, B., Sickmann, A., Pfanner, N., & Meisinger, C. (2011) Regulation of mitochondrial protein import by cytosolic kinases. *Cell* **144,** 227–239.
14. Thompson, J. D, Higgins, D. G., Gibson, T. J. (1994) CLUSTAL W: improving the sensitivity of progressive multiple sequence alignment through sequence weighting, position-specific gap penalties and weight matrix choice. *Nucleic Acid Res.* **22**,4673–4680.
15. Kouza, M., Faraggi, E., Kolinski, A., & Kloczkowski, A. (2017) The GOR Method of Protein Secondary Structure Prediction and Its Application as a Protein Aggregation Prediction Tool. *Methods in Mol. Biol. (Clifton, N.J.)* **1484**, 7–24.
16. Nielsen H. (2017). Predicting Secretory Proteins with SignalP. *Methods Mol. Biol. (Clifton, N.J.)* **1611**, 59–73.
17. Blom, N., Gammeltoft, S., & Brunak, S. (1999). Sequence and structure-based prediction of eukaryotic protein phosphorylation sites. *J. Mol. Biol.* **294**, 1351–1362.
18. Guex, N., & Peitsch, M. C. (1997). SWISS-MODEL and the Swiss-PdbViewer: an environment for comparative protein modeling. *Electrophoresis* **18**, 2714–2723.
19. Schwede, T., Kopp, J., Guex, N., & Peitsch, M. C. (2003). SWISS-MODEL: An automated protein homology-modeling server. *Nucleic acids Res.* **31**, 3381–3385.
20. Jendele, L., Krivak, R., Skoda, P., Novotny, M., & Hoksza, D. (2019). PrankWeb: a web server for ligand binding site prediction and visualization. *Nucleic acids Res*. **47**(W1), W345–W349.
21. Tokmakov, A. A., Iguchi, S., Iwasaki, T., & Fukami, Y. (2011). Unfertilized frog eggs die by apoptosis following meiotic exit. *BMC Cell Biol*. **12**:56.
22. Iguchi, S., Iwasaki, T., Fukami, Y., & Tokmakov, A. A. (2013). Unlaid Xenopus eggs degrade by apoptosis in the genital tract. *BMC Cell Biol*. **14**:11.